EFDA–JET–PR(09)32

Y. Sun, Y. Liang, H.R. Koslowski, S. Jachmich, A. Alfier, O. Asunta, G. Corrigan, C. Giroud, M.P. Gryaznevich, D. Harting, T. Hender, E. Nardon, V. Naulin, V. Parail, T. Tala, C. Wiegmann, S. Wiesen and JET EFDA contributors

Toroidal Rotation Braking with $n = 1$ Magnetic Perturbation Field on JET

Toroidal Rotation Braking with $n = 1$ Magnetic Perturbation Field on JET

Y. Sun[1], Y. Liang[1], H. R. Koslowski[1], S. Jachmich[2], A. Alfier[3], O. Asunta[4], G. Corrigan[5], C. Giroud[5], M. P. Gryaznevich[5], D. Harting[1], T. Hender[5], E. Nardon[5], V. Naulin[6], V. Parail[5], T. Tala[7], C. Wiegmann[1], S. Wiesen[1] and JET EFDA contributors*

JET-EFDA, Culham Science Centre, OX14 3DB, Abingdon, UK

[1]Institute for Energy Research – Plasma Physics, Forschungszentrum Jülich, Association EURATOM-FZJ, Trilateral Euregio Cluster, 52425 Jülich, Germany
[2]Association EURATOM-Belgian State, Koninklijke Militaire School-Ecole Royale Militaire, Trilaterial Euregio Cluster, B-1000 Brussels, Belgium
[3]Associazione EURATOM-ENEA sulla Fusione, Consorzio RFX Padova, Italy
[4]Association EURATOM-Tekes, Helsinki University of Technology, P.O. Box 4100 FI-02015 TKK, Finland
[5]EURATOM-UKAEA Fusion Association, Culham Science Centre, Abingdon, OX14 3DB, UK
[6]Association EURATOM–Risø National Laboratory, OPL-128 Risø, DK-4000 Roskilde, Denmark
[7] Association EURATOM-Tekes, VTT, P.O. Box 1000, FIN-02044 VTT, Finland(Footnotes)
[*] See annex of F. Romanelli et al, "Overview of JET Results", (Proc. 22 [nd] IAEA Fusion Energy Conference, Geneva, Switzerland (2008)).*

Preprint of Paper to be submitted for publication in
Plasma Physics and Controlled Fusion

ABSTRACT.

A strong toroidal rotation braking has been observed in plasmas with application of an $n = 1$ magnetic perturbation field on JET tokamak. Calculation results from the momentum transport analysis show that the torque induced by the $n = 1$ perturbation field has a global profile. The maximal value of this torque is at the plasma core region ($\rho < 0.4$) and it is about half of the **N**eutral **B**eam **I**njection (NBI) torque. The **N**eoclassical **T**oroidal **V**iscosity (NTV) torque is calculated in different collisionless regimes. This observed torque profile agrees well with the predicted NTV torque in the ν regime with the collisional boundary layer effect included.

1. INTRODUCTION.

Helical magnetic perturbation field with a toroidal mode number up to 3 have been applied for either active control or suppression of the Edge Localized Modes (ELMs) in H-mode plasmas on several tokamaks [1,2,3], and it are planed to be applied on ITER [4]. However, both, resonant [5] and non-resonant [6,7] components of the perturbation field can influence on the plasma rotation. It was well known that the plasma rotation is a significant concern for the control of the MHD instabilities in a tokamak, because of its stabilising effects on Resistive Wall Modes (RWMs) [8] and **N**eoclassical **T**earing **M**odes (NTMs) [9]. Therefore, understanding of the plasma braking mechanism with a helical magnetic perturbation becomes an important issue for an optimisation for the application of magnetic perturbations.

The **N**eoclassical **T**oroidal **V**iscosity (NTV) theory has been developed by Shaing to describe the effects of the non-axisymmetric magnetic perturbations on the plasma rotation in the collisionless [6] and plateau [10] regimes. The collisionless regime can be further divided into two main regimes: the regime and the ν regime [6]. The breaking of the toroidal magnetic symmetry due to application of the non-axisymmetric magnetic perturbations causes a non-ambipolar radial particle flux and hence the NTV. A generalized analytic result of NTV has been presented by Park [11]. The influence of the NTV torque on the field penetration process has been investigated by Cole [7]. A neoclassical 'offset' rotation has been predicted by the NTV theory [6, 7].

Recently, a good agreement between the calculated torque from NTV theory in the $1/\nu$ regime and the observed torque induced by the $n = 3$ magnetic perturbation has been reported on NSTX [12]. The observed rotation damping time on DIII-D was close to the NTV damping time in the $1/\nu$ regime, and NTV damping time in the ν regime is at least two orders of magnitude larger [13]. However, it was shown that the plasma in DIII-D was mainly in the ν regime. The plasma in ITER is also expected to be in the ν regime. The enhancement of the NTV torque in the ν regime has been predicted by including the collisional boundary layer effect [14]. The NTV torque from the boundary layer contribution scales like $\sqrt{\nu}$. The bounce resonance can also enhance the transport [11]. The existence of the neoclassical 'offset' rotation with $n = 3$ perturbation field was observed on DIII-D [15]. Strong global magnetic braking effect has been observed in ELMs control experiment with magnetic perturbation field generated by the **E**rror **F**ield **C**orrection **C**oils (EFCCs) on JET [16].

The torque induced by the $n = 1$ magnetic perturbation on JET is analyzed and compared with the torque predicted by the NTV theory in this paper. The paper is organized as follows: The torque with application of the $n = 1$ magnetic field perturbation on JET, T_{EFCC}, is determined by momentum transport analysis using the JETTO code [17] in Sec.2. The NTV torque profile is calculated and compared with T_{EFCC} in Sec. 3, followed by the discussion and summary of the main results in Sec. 4.

2. DETERMINATION OF THE TORQUE INDUCED BY THE MAGNETIC PERTURBATION ON JET.

The torque with application of the $n = 1$ magnetic field perturbation on JET is determined by momentum transport analysis using the JETTO code and the least-square fitting technique in this part.

2.1 MOMENTUM TRANSPORT EQUATION

The angular momentum transport equation in the JETTO code can be written as

$$\frac{\partial}{\partial t}\left(\left\langle R^2\right\rangle \sum_{ions} n_j m_j \omega\right) + fA\,\frac{1}{\rho}\frac{\partial}{\partial \rho}\left[\rho\,\frac{\left\langle R^2\right\rangle}{fA}\sum_{ions}\left(m_j \omega \Gamma_j^p + \Gamma_j^\omega\right)\right] = T^\phi \qquad (1)$$

where R is the major radius, $\langle ... \rangle$ denotes the flux surface average, Σ denotes the sum over all ion species, n_j and m_j are the density and mass of the ion species, respectively. $\omega = V_\phi / R$ is the angular rotation frequency and V_ϕ is the torodial rotation velocity, $f = RB_\phi$ and B_ϕ is the toroidal magnetic field, $A = \langle 1/R^2 \rangle$ is a geometrical quantity, $\rho \equiv \sqrt{\psi_T/\pi B_0}$ is the flux-surface label, ψ_T is the toroidal flux, T^ϕ is the source torque, Γ_j^p and Γ_j^ω are the ion particle flux and angular momentum flux, respectively, defined as

$$\Gamma_j^p = -\left(D_j\left\langle\left|\nabla\rho\right|^2\right\rangle\frac{\partial n_j}{\partial\rho} + \left\langle\left|\nabla\rho\right|\right\rangle V_{p,j} n_j\right),$$

and

$$\Gamma_j^\omega = -m_j n_j\left(\chi_M\left\langle\left|\nabla\rho\right|^2\right\rangle\frac{\partial\omega}{\partial\rho} + \left\langle\left|\nabla\rho\right|\right\rangle V_{inwm}\omega\right),$$

D_j and $V_{p,j}$ are the ion particle diffusion coefficient and pinch velocity profiles, respectively, χ_M and V_{inwm} are momentum diffusion coefficient and pinch velocity profiles, respectively. The particle flux is neglected in the following analysis. Then, the momentum transport equation can be written as:

$$C_1\frac{\partial\gamma}{\partial t} = \frac{1}{\rho}\frac{\partial}{\partial\rho}\rho\left(C_2\frac{\partial\gamma}{\partial\rho} + C_3\gamma\right) + S \qquad (2)$$

where

$$\gamma = \rho_i\omega,\ \rho_i = \sum_{ions} n_j m_j,\ C_1 \equiv \frac{\left\langle R^2\right\rangle}{fA}, \qquad C_2 \equiv C_1\left\langle\left|\nabla\rho\right|^2\right\rangle\chi_M,$$

$C_3 \equiv C_1\left(-\left\langle|\nabla\rho|^2\right\rangle\left(\frac{\partial \ln \rho_i}{\partial \rho}\right)\chi_M + \left\langle|\nabla\rho|\right\rangle V_{inwm}\right)$ and $S \equiv \frac{T^{\phi}}{fA}$. The momentum evolution can be simulated using Equation 2 with known χ_M, V_{inwm} and all the momentum sources S.

2.2. METHOD TO DETERMINE THE MOMENTUM DIFFUSION COEFFICIENT AND PINCH VELOCITY PROFILE

The toroidal plasma rotation velocity, measured by Charge eXchange Recombination Spectroscopy (CXRS), shows a 50% reduction with an n=1 magnetic perturbation for JET Pulse No: 75342 in Figure 1. The spatial profiles of the plasma angular rotation, ion temperature, electron density and electron temperature (with (triangles) and without (circles) perturbation field) are shown in Figure 2. During the application of the magnetic perturbation, there is a slightly change of the ion temperature in the plasma core region. There is no significant change of the other parameters, such as the electron density and temperature, the normalized plasma beta (the ratio between the thermal pressure and magnetic pressure), and q_{95} (the safety factor at normalized poloidal magnetic flux of 0.95) as also shown in Figure 1 and Figure 2. The maximal amplitude of the perturbation field for this pulse is only about 0.1-0.2% of the toroidal magnetic field strength. The Fourier spectrum of the n=1 **R**esonant **M**agnetic **P**erturbation (RMP) [18] is shown in Figure 3. The dashed line shows the resonant condition m=nq. It shows that there are strong non-resonant ($m \neq nq$) components in the perturbation field induced by the EFCCs.

By using Eq. (2), the χ_M and V_{inwm} profiles are obtained by fitting the observed velocity evolution after the switch-off of the EFCC current. At this stage, the only source term is the NBI torque, which is calculated by the PENCIL code [19]. The Polynomial functions are used as base functions, $\chi_M \equiv \sum_{n=0}^{N} \alpha_n \rho^n$, here $V_{inwm} \equiv \sum_{m=0}^{M} \beta_m \rho^m$ α, β are the unknown free parameters to be fitted, N and M are the orders of the Polynomial base functions.

3.3. CALCULATION OF THE TORQUE INDUCED BY THE N=1 MAGNETIC PERTURBATION

With the application of the magnetic perturbation from the EFCCs, an additional torque will be exerted on the plasma. The torque during the flat top phase of the EFCC current, T_{EFCC}, is calculated by solving Eq.2 with the other terms determined by momentum transport analysis above.

Figure 4 shows the obtained T_{EFCC} ($-T_{\mathrm{EFCC}}$ is plotted in the figure) profiles by using different χ_M and V_{inwm} profiles fitted from different base functions described above. Two of them do not consider the pinch velocity in momentum flux with N = 4 (triangles) and N = 6 (diamonds), and the other two consider the pinch velocity with M = N = 4 (circles) and M = N = 6 (pentacles). In these calculations the pinch velocities changes in a large range (0~20 m/s). However, the obtained torque profile does not show a significant change.

The obtained torque profile is not very sensitive to the selected set of base functions, because it

is mainly determined by the change of the total momentum flux due to the magnetic perturbation. To separate the individual effect of χ_M and V_{inwm} is beyond the discussion of this paper.

The obtained torque in the plasma core region is about half of the NBI torque. The maximum torque is in the plasma core region ($\rho < 0.4$), while it is found to be closer to the edge on NSTX [12] and DIII-D [15], both using a higher *n* perturbation field. *dL*/*dt* (dashed dotted line) at the time just after the switch-off of the EFCC current, where *L* is the angular momentum density, is also shown in Figure 4. It is a first order estimation of the torque profile with the application of the magnetic perturbation, which is similar to the method used on NSTX [12] and DIII-D [15]. The profile has similar shape to the obtained torque profile, but different by 40-50% in absolute values.

The obtained T_{EFCC} has a global profile. It is not localized at certain magnetic surfaces. The evolution of the plasma rotation is obviously different from the mode locking process as also found on NSTX [12] and DIII-D [15]. This suggests that this torque may not be caused by the resonant electromagnetic braking. The NTV torque may be a good candidate to explain this observed torque.

With the assumption that $T_{EFCC} \propto \tilde{B}^2 \propto I^2_{EFCC}$, where $\tilde{B}$ is the magnetic field perturbation and $\mathrm{I_{EFCC}}$ is the EFCC current, the simulation of the momentum transport equation can well reproduce the observed evolution of the plasma rotation as shown in Figure 5. This is also a check of the correctness of the fitting process and the obtained torque profile.

3. COMPARISON WITH NTV TORQUE.

3.1 NTV THEORY

The toroidal symmetry breaking, induced by the non-axisymmetric magnetic perturbation, will cause a nonambipolar radial particle flux. The radial currents of the nonambipolar diffusion will cause a toroidal viscosity, which is called NTV [6]. This viscosity is equivalent to a torque which is called NTV torque.

The magnetic field strength |B| can be written as

$$\begin{aligned} B &= B_0\left(1-\varepsilon\cos\theta\right)+B_0\sum_n\left[A_n\left(\theta\right)\cos\left(n\zeta_0\right)+B_n\left(\theta\right)\sin\left(n\zeta_0\right)\right] \\ &= B_0\left(1-\varepsilon\cos\theta\right)+B_0\sum_{(m,n)\neq(0,0)} b_{nmc}\cos\left(m\theta-n\zeta\right)+b_{nms}\sin\left(m\theta-n\zeta\right) \end{aligned} \tag{3}$$

where B_0 is the magnetic field strength on the magnetic axis, is the amplitude of the component, *n* is the toroidal mode number of the helical perturbation, $\zeta_0 = q\theta - \zeta$, *q* is the safety factor, θ and ζ are the poloidal and toroidal angles, respectively, in Hamada coordinate. The calculation of the Hamada coordinates is discussed in Appendix A.

The relationship between (A_n, B_n) and (b_{nmc}, b_{nms}) can be obtained from Equation (3) as follows,

$$\begin{cases} A_n\left(\theta\right)=\sum_m\left[b_{nmc}\cos\left(\left(m-nq\right)\theta\right)+b_{nms}\sin\left(\left(m-nq\right)\theta\right)\right] \\ B_n\left(\theta\right)=\sum_m\left[-b_{nmc}\sin\left(\left(m-nq\right)\theta\right)+b_{nms}\cos\left(\left(m-nq\right)\theta\right)\right] \end{cases} \tag{4}$$

The variation of the magnetic field strength should be evaluated on the distorted magnetic surface [6], which means the Lagrangian variation in the field strength should be calculated [20]. This Lagrangian variation in the magnetic field strength is given by

$$\delta_L B = \delta_E B + \delta_\xi B \tag{5}.$$

Here, $\delta_E B$ is the Eulerian variation in the magnetic field strength and $\delta_\xi B$ is the variation of the magnetic field strength due to the displacement of the magnetic surface. The calculation of the variation in the magnetic field strength is discussed in Appendix B. The results on NSTX showed that the NTV torque due to the displacement of the magnetic surface is dominant [20].

The collisionless regime ($\nu/\varepsilon < \sqrt{\varepsilon\omega_t}$, here ν is the collisionality, $\omega_t = v_t/R_0 q$ is the transit frequency and $v_t = (2T/m)^{1/2}$ is the thermal velocity) can be further divided into two main regimes according to the relationship between the values of the collisionality ν and $\vec{E}\times\vec{B}$ drift frequency $\omega_E = \frac{E_\rho}{\rho B_0}$ (here E_ρ is the radial electrical field). One is the $1/\nu$ ($q\omega_E < \nu/\varepsilon < \sqrt{\varepsilon\omega_t}$) regime and the other is the ($q\omega_E > \nu/\varepsilon$) regime. The names of the regimes indicate the dependence of the transport on the collisionality. The reduction of the transport in the regime comes from the electric drift effect. In the regime, a collisional boundary layer condition (the boundary between the trapped and untrapped particles) is introduced to remove the singularity in the pitch angle integration [14]. By including this new physics, it was found that the NTV contribution from the boundary layer, scaling as $\sqrt{\nu}$, is larger than the contribution from the main trapped particles in this regime as discussed in [14] and will be shown in the following.

According to the NTV theory [6, 14], the NTV torque in the different collisionless regimes (the $1/\nu$ regime, the ν regime contributed from main trapped particles and the boundary layer) from the ions (the ions viscosity is $(m_i/m_e)^{1/2}$ times larger than the electron viscosity) can be rewritten in

$$T_{NTV} = -\tau_{NTV,i}^{-1}\left\langle R^2\right\rangle\left(\gamma - k_{c,i}\gamma_{NC0}\right) \tag{6}$$

$$\text{here } \tau_{NTV,i}^{-1} \approx \begin{cases} 1.23R_0^2\left\langle\frac{1}{R^2}\right\rangle q^2\frac{\omega_{ti}^2}{\nu_i}I_\lambda & \left(1/\nu \quad regime\right) \\ 0.13R_0^2\left\langle\frac{1}{R^2}\right\rangle\frac{\nu_i\omega_{ti}^2}{\omega_E^{\,2}}G_\lambda & \left(\nu \quad regime\right) \\ 0.064R_0^2\left\langle\frac{1}{R^2}\right\rangle\left[\ln\left(64q\varepsilon\omega_E/\nu_i\right)\right]^{1/2}\frac{q^2\omega_{ti}^2\sqrt{\nu_i}}{\left(\left|q\omega_E\right|\right)^{3/2}}H_\lambda & \left(\nu \quad regime,bdy\right) \end{cases} \tag{7}$$

$$k_{c,i} \approx \begin{cases} 3.54 & \left(1/\nu \quad regime\right) \\ 0.92 & \left(\nu \quad regime\right) \\ 1.53 & \left(\nu \quad regime,bdy\right) \end{cases} \tag{8}$$

$\omega_{ti} = \nu_{ti}/R_0 q$ is the ion transit frequency and $\nu_{ti} = (2T_i/m_i)^{1/2}$ is the ion thermal velocity,

$\nu_i = \frac{e_0^4}{8\sqrt{2}\pi\varepsilon_0^2}\frac{N_i Z_i^4 \ln\Lambda}{\left(m_i^{1/2}T_i^{3/2}\right)}$ is the ion collisionality, I_λ(defined in [6]), G_λ(defined in [14]) and H_λ are the pitch angle integrations (they are discussed in Appendix C), which are proportional to B and mainly determined by the spectrum of the magnetic perturbation, γ_{NC0} is defined as $\gamma_{NC0} \equiv \rho_i \frac{V_{NC0}}{R} = \rho_i \frac{q}{e_i \rho B_0} \frac{dT_i}{d\rho}$, $V_{NC} \equiv k_{c,i} V_{NC0}$ and is the so called 'offset' neoclassical velocity, ν is the coefficient of the neoclassical velocity, $k_{c,i}$ denotes the contribution from boundary layer in the regime . In the calculation of $k_{c,i}$, one neoclassical coefficient 1.17 is taken for the contribution from the poloidal flow [21]. The calculated $k_{c,i}$ for the boundary layer contribution is close to the observed value (between 1 and 2) on DIII-D [15].

3.2. NTV TORQUE CALCULATION AND COMPARISON WITH THE OBSERVED TORQUE T_{EFCC}

The profiles of the transit ($\varepsilon^{1/2}\omega_{ti}$, dotted dashed line), $\vec{E}\times\vec{B}$ drift ($|q\omega_E|$, dashed line) and collision (ν_i/ε, solid line) frequencies for ions are shown in Figure 6. The radial electrical field is calculated from the radial force balance equation in the JETTO code by using the poloidal flow calculated by the NCLASS code [22]. It shows that the plasma is mainly in the regime near the plasma core region, which is similar to DIII-D and ITER [13].

The vacuum field superposition is used in the NTV torque calculation. The calculation of the variation of the magnetic field strength is discussed in Appendix B. The calculated NTV torque from the Eularian variation in the magnetic field strength is shown in Figure 7. The triangles are the NTV torque in the $1/\nu$ regime, the diamonds are the torque contributed from the main trapped particles in the ν regime and the circles are the torque contributed from the boundary layer in the regime. The calculated NTV torque profile in the $1/\nu$ regime agrees well with the observed torque profile T_{EFCC}. In the ν regime, the NTV torque contributed from the boundary layer is the dominant component as pointed out by Shaing [14]. The NTV torque in the regime without boundary layer contribution is much smaller the observed torque, which is similar to the results from DIII-D [13]. The NTV torque contributed from the boundary layer in the regime is closer to the observed torque than the NTV torquecontributed from the main trapped particles in the regime. However, it is still smaller than the observed torque.

The calculated NTV torque from the Lagrangian variation in the magnetic field strength is shown in Figure 8. It shows that the NTV torque from the Lagrangian variation in the magnetic field strength is much larger than that from the Eularian part. In the plasma core region, the NTV torque in the $1/\nu$ regime is about 4 times larger than the observed torque, while the NTV torque contributed from the boundary layer in the ν regime is much closer to the observed torque. There is one peak at about $\rho = 0.53$ in the NTV torque profile. This peak corresponds to the location of the $q = 2$ surface. With the vacuum field assumption, there is a big 2/1 island inside the plasma. Because the NTV torque near the island region is proportional to $\tilde{B}$ [23], the islands will give a larger contribution to

the NTV than that from the non-resonant component (proportional to $\tilde{B}^2$). However, the resonant components of the perturbation field strongly depend on the plasma response.

With the assumption that all the resonant components of the perturbation field are screened by the plasma response, the NTV torque contributed from the non-resonant component is shown in Figure 9. It shows that there is a significant reduction of the NTV torque near $\rho = 0.53$ region, which means that the large NTV torque in that region is mainly due to the island. In the plasma core region, there is no significant change of the NTV torque, which means that the NTV torque in this region is mainly contributed from the non-resonant components of the magnetic perturbation. In the plasma core region, the NTV torque contributed from the boundary layer in the ν regime agrees well with the observed torque.

Figure 10 shows the neoclassical 'offset' angular momentum density (dashed) in Eq. 5. It is determined by the ion temperature gradient. It shows that the 'offset' rotation is comparable to the plasma rotation in the plasma core region. Therefore, it should not be neglected in this calculation. Figure 11 shows the contributions from different harmonics of the magnetic perturbation to the pitch angle integration . The contribution from the $n = 1$ magnetic perturbation is dominant. This is mainly determined by the characteristics of the EFCC coils. It is different from the result on NSTX [12], in which the contribution from $n = 5$ has been found to be dominant.

5. DISCUSSION AND CONCLUSION.

The torque profile with the application of the $n = 1$ magnetic perturbation on JET, T_{EFCC}, is determined by momentum transport analysis using the JETTO code. The NBI torque is calculated by the PENCIL code. The perpendicular diffusion coefficient and pinch velocity profile are determined by fitting the evolution of the velocity after the switch-off of EFCC current.

The T_{EFCC} has a global profile. The maximal torque is in the plasma core region, which is different from the observations on NSTX and DIII-D with higher n perturbation field. This torque is not localized at a certain rational surface and the velocity evolution is obviously different from that in the mode locking phase as also observed on NSTX. Therefore, it seems not to be induced by resonant electromagnetic braking effect.

With the assumption that $T_{EFCC} \propto \tilde{B}^2$, the simulation of the momentum transport equation can well reproduce the observed evolution of the plasma rotation. This $\tilde{B}^2$ dependence is in agreement with the non-resonant NTV theory.

With the vacuum field superposition, the NTV torque profiles in different collisionless regimes are calculated and compared with the observed torque T_{EFCC}. The contribution from $n = 1$ magnetic perturbation to the NTV torque is dominant in this $n = 1$ EFCCs configuration.

The calculated NTV torque profile caused by the Eulerian variation in the magnetic field strength in the $1/\nu$ regime agrees well with the T_{EFCC} profile. The NTV torque contributed from the boundary layer in the ν regime is still smaller than the observed torque, although it is much closer to the observed torque than the NTV torque contributed from the main trapped particles in the ν regime.

However, the calculation shows that the plasma in the core region is mainly in the ν regime.

By including the effect of the displacement of the magnetic surface, the NTV torque in the core region caused by the Lagrangian variation of the magnetic field strength contributed from the boundary layer in the ν regime agrees well with the observed torque. Therefore, the NTV theory agrees very well with the experimental observation with n=1 magnetic perturbation on JET.

Even if all the resonant components of the perturbation field are assumed to be screened, the NTV torque in the core region does not change much, which means that the NTV torque in the plasma core region is mainly caused by the non-resonant components of the perturbation field. The plasma response may change both resonant and non-resonant components of the perturbation field. However, the non-resonant components of the perturbation field are not so sensitive to the plasma response as the resonant components. Therefore, the results will not significantly change, even if we consider the plasma response. The perturbed 3D equilibrium calculation with real plasma response is necessary to get accurate magnetic perturbation on distorted flux surfaces in the future. How to get the real plasma response is under investigation elsewhere.

The plasma response, such as Resonant Field Amplification (RFA) effect of the external kink modes and the screening effects of the plasma rotation, should be included in future investigations. The resonant braking effects from the NTV or electromagnetic torque strongly depend on the plasma response. It should also be investigated, after the plasma response is obtained.

ACKNOWLEDGEMENT.

The authors would like to acknowledge helpful discussions with K.C. Shaing, Y. Liu, D. Howell, V. D. Pustovitov, M. J. Schaffer and J. Park. This work, supported by the European Communities under the contract of Association between EURATOM and FZJ, was carried out within the framework of the European Fusion development Agreement. The views and opinions expressed herein do not necessarily reflect those of the European Commission.

REFERENCES

[1]. Y. Liang et al., Physical Review Letters **98**, 265004 (2007)
[2]. T. Evans et al., Physical Review Letters **92**, 235003 (2004)
[3]. S.J. Fielding et al., Europhysics Conference Abstract **25**A, 1825 (2001)
[4]. M.J. Schaffer et al., Nuclear Fusion **48** 024004 (2008)
[5]. R. Fitzpatrick, Physics of Plasmas **5**, 3325(1998)
[6]. K.C. Shaing, Physics of Plasmas **10**, 1443(2003)
[7]. A.J. Cole et al., Phys. Plasmas **15**, 056102 (2008)
[8]. E.J. Strait et al., Physical Review Letters **74**,2483 (1995)
[9]. R. Buttery et al., Physics of Plasmas **15**, 056115 (2008)
[10]. K.C. Shaing et al., Physics of Plasmas **29**, 521 (1986)
[11]. J. Park et al., Physical Review Letters **102**, 065002 (2009)

[12]. W. Zhu et al., Physical Review Letters **96**, 225002 (2006)
[13]. M. BÈcoulet et al., Nuclear Fusion **49** 085011 (2009)
[14]. K.C. Shaing, Physics of Plasmas **15**, 082506 (2008)
[15]. A.M. Garofalo et al., Physical Review Letters **101**, 195005 (2008)
[16]. Y. Liang et al, 22nd IAEA Fusion Energy Conference, October 13-18, 2008, Geneva, EX/4-2
[17]. G. Cenacchi and A. Taroni, (1988) "JETTO: A Free-Boundary Plasma Transport Code (Basic Version)", JET Report JET-IR(88)03
[18]. M. BÈcoulet et al., Nuclear Fusion **48** 024003 (2008)
[19]. C.D. Challis et al., Nuclear Fusion **29** 563 (1989)
[20]. J. Park et al., Phys. Plasmas **16**, 056115 (2009)
[21]. K.C. Shaing, Phys. Plasmas **14**, 024501 (2007)
[22]. W.A. Houlberg, *et al*., Physics of Plasmas **4** 3230 (1997)
[23]. K.C. Shaing, Physical Review Letters **87**, 245003 (2001)
[24]. R.C. Grimm et al., Journal Computational Physics **49**, 94 (1983)
[25]. V.D. Pustovitov, Plasma Phyics Reports, **24**, 510 (1998)

APPENDIX A. CALCULATION OF THE HAMADA COORDINATES

Hamada coordinates are calculated by using two methods described in [24,25]. These two methods are essentially equivalent.

The magnetic field can be written in

$$\vec{B} = q\nabla\psi\times\nabla\theta - \nabla\psi\times\nabla\zeta \tag{A1}$$

here (ψ, θ, ζ) is a right-handed straight field line coordinate system. According to the calculation in [24, 25], the Hamada coordinates (θ, ζ) can be obtained by

$$\begin{cases} \theta = \alpha\int_l \dfrac{R}{|\nabla\psi|}dl \\ \zeta = \phi - \int_l \dfrac{R}{|\nabla\psi|}\left(B_T R^{-1} - \alpha q\right)dl \end{cases} \tag{A2}$$

here $\alpha(\psi) = 2\pi/\oint_1 \frac{R}{|\nabla\psi|}\,dl$, B_T is the toroidal magnetic field strength, and the integrations are taken along the poloidal contour l of the magnetic surface.

The calculated Hamada coordinates for JET Pulse No: 75342 at t=24s are shown in Figure A1 and A2. Figure A1 shows the equally spaced grid (ψ, θ) in Hamada coordinates. Figure A2 shows the (θ, ζ) in Hamada coordinates on the surface. $\sqrt{\psi} = 0.95$ The directions of the covariant coordinates (e_θ, e_ζ) and contravariant coordinates (e^θ, e^ζ) are marked in this figure.

APPENDIX B. CALCULATION OF THE VARIATION OF THE MAGNETIC FIELD STRENGTH WITH THE VACUUM SUPERPOSITION

The magnetic field perturbation profile induced by EFCCs is calculated by using Biot-Savart laws.

The variation of the magnetic field strength along the perturbed magnetic field lines is called Lagrangian variation in field strength and is given by [20],

$$\delta_L B = \delta_E B + \delta_\xi B \tag{B1}$$

The first term in the right-hand side of Eq. (B1) is the Eularian variation

$$\delta_E B = \vec{\tilde{B}} \cdot \frac{\vec{B}}{B} = \tilde{B}_{//} \tag{B2}$$

here B is the perturbation field induced by the EFCC. The second term is the contribution from the displacement of the magnetic surface due to the perturbation field,

$$\delta_\xi B = \vec{\xi} \cdot \nabla B \approx -\frac{B_0}{R_0} \xi_R \tag{B3}$$

here ξ_R is the magnetic surface displacement in the major radius direction.

With vacuum field superposition, the displacement of the magnetic surface in the major radius direction due to the perturbation field can be written as:

$$\nabla_{//} \xi_R = \frac{d\xi_R}{dl} = \frac{\vec{\tilde{B}} \cdot \nabla R}{B} = \frac{B^R}{B} \tag{B4}$$

here

$$\nabla_{//} = \frac{\vec{B}}{B} \cdot \nabla = \frac{B^\varsigma}{B} \left(\frac{1}{q} \partial_\theta + \partial_\varsigma \right)$$

From Eqs. B3 and B4, it is obtained

$$\left(\frac{1}{q} \partial_\theta + \partial_\varsigma \right) \frac{\delta_\xi B}{B_0} = B_1 \tag{B5}$$

here B1 = $-\frac{B^R}{R_0 B^\zeta}$. The variation of the magnetic field strength due to the displacement of the magnetic surface can be obtained by integrating Eq. B5 along the magnetic field line.

Using Fourier expansion $\frac{\delta_\xi B}{B_0} = \sum_{m,n} b^\xi_{mn} e^{i(m\theta - n\varsigma)}$ and $B_1 = \sum_{m,n} \tilde{b}^R_{mn} e^{i(m\theta - n\varsigma)}$, it is found

$$b^\xi_{mn} = \frac{\tilde{b}^R_{mn}}{i\left(\frac{m}{q} - n \right)} \tag{B6}$$

There is a singularity at the rational surface $q = m/n$, if $\tilde{b}^R{}_{mn} \neq 0$, if on the rational surface (there is an island). This is valid outside the island separatrix. For the non-resonant component $\left| \frac{m}{n} - n \right|$ O (1)

$\tilde{b}^R_{mn}$ the scaling of the magnetic field strength variation will be $\delta_\zeta B \propto \tilde{B}$ and the resultant NTV torque will be $T \propto \tilde{B}^2$. For the resonant component near the island region, the displacement will be the island width, which is proportional to $\sqrt{\tilde{B}}$. Therefore, the scaling of the magnetic field strength variation will be $\delta_\zeta B \propto \sqrt{\tilde{B}}$ and the resultant NTV torque will be $T \propto \tilde{B}$, as shown in [23]. This torque will be much larger than the non-resonant component NTV torque and it is localized near the island region. However, this component will strongly depend on the plasma response.

Using Fourier expansion $\frac{\delta_L B}{B_0} = \sum_{m,n} b^L_{mn} e^{i(m\theta - n\zeta)}$ and $\frac{\delta_E B}{B_0} = \sum_{m,n} b^E_{mn} e^{i(m\theta - n\zeta)}$ the spectrum of the Lagrangian variation of the magnetic field strength can be written in

$$b^L_{mn} = b^E_{mn} + b^\xi_{mn} \tag{B7}$$

APPENDIX C. PITCH ANGLE INTEGRATIONS IN NTV TORQUE CALCULATION

According to the NTV theory [6, 14] the pitch angle integrations can be written in

$$\begin{cases} I_\lambda = \dfrac{\varepsilon^{3/2}}{\sqrt{2}} \int_0^1 d\kappa^2 F(\kappa) \left[E(\kappa) - \left(1-\kappa^2\right) K(\kappa) \right]^{-1} \\ G_\lambda = \dfrac{1}{\sqrt{32\varepsilon}} \int_0^1 d\kappa^2 \left[E(\kappa) - \left(1-\kappa^2\right) K(\kappa) \right] \sum_n \left(\alpha_n^2 + \beta_n^2 \right) \\ H_\lambda = \left\{ \sum_n \sqrt{n} \left(\alpha_{bn}^2 + \beta_{bn}^2 \right) \right\} \end{cases} \tag{C1}$$

here $$F(\kappa) = \sum_n n^2 \left\{ \left[\int d\theta \left(\kappa^2 - \sin^2(\theta/2) \right)^{1/2} A_n \right]^2 + \left[\int d\theta \left(\kappa^2 - \sin^2(\theta/2) \right)^{1/2} B_n \right]^2 \right\}$$

$$\begin{cases} \alpha_n = \dfrac{\partial}{\partial \kappa^2} \left\{ \int d\theta \dfrac{(-1/2)}{K(\kappa)\sqrt{\kappa^2 - \sin^2(\theta/2)}} \left[A_n(\theta) \left(1 - e^{-\sqrt{n}y} \cos(\sqrt{n}y) \right) + B_n(\theta) e^{-\sqrt{n}y} \sin(\sqrt{n}y) \right] \right\} \\ \beta_n = \dfrac{\partial}{\partial \kappa^2} \left\{ \int d\theta \dfrac{(-1/2)}{K(\kappa)\sqrt{\kappa^2 - \sin^2(\theta/2)}} \left[B_n(\theta) \left(1 - e^{-\sqrt{n}y} \cos(\sqrt{n}y) \right) - A_n(\theta) e^{-\sqrt{n}y} \sin(\sqrt{n}y) \right] \right\} \end{cases}$$

$$\begin{cases} \alpha_{bn} = \left. \int d\theta \dfrac{A_n(\theta)}{K(\kappa)\sqrt{\kappa^2 - \sin^2(\theta/2)}} \right|_{1-\Delta\kappa^2} \\ \beta_{bn} = \left. \int d\theta \dfrac{B_n(\theta)}{K(\kappa)\sqrt{\kappa^2 - \sin^2(\theta/2)}} \right|_{1-\Delta\kappa^2} \end{cases}, \qquad \Delta\kappa^2 = \left[\frac{\nu_{*d}}{\ln\left(16/\sqrt{\nu_{*d}}\right)} \right]^{1/2}$$

$$y = \left(1-\kappa^2\right) \left(\frac{\nu_D}{\nu_i} \right)^{-1/2} \left[\frac{\nu_{*d}}{\ln\left(16/\sqrt{\nu_{*d}}\right)} \right]^{-1/2}, \qquad \nu_{*d} \approx 4 \frac{\nu_i/\varepsilon}{q\omega_E} \qquad \rightarrow$$

$E(\kappa)$ and $K(\kappa)$ are elliptic integrations, v_D is the deflection frequency. Neglecting the energy

dependence of v_D, $(v_D/v_i)^{-1/2} \approx 1$. The pitch angle integrations have $\tilde{B}^2$ dependence. They are mainly determined by the spectrum of the perturbation field. In the ν regime, they also depend on the collisionality and electric drift frequency.

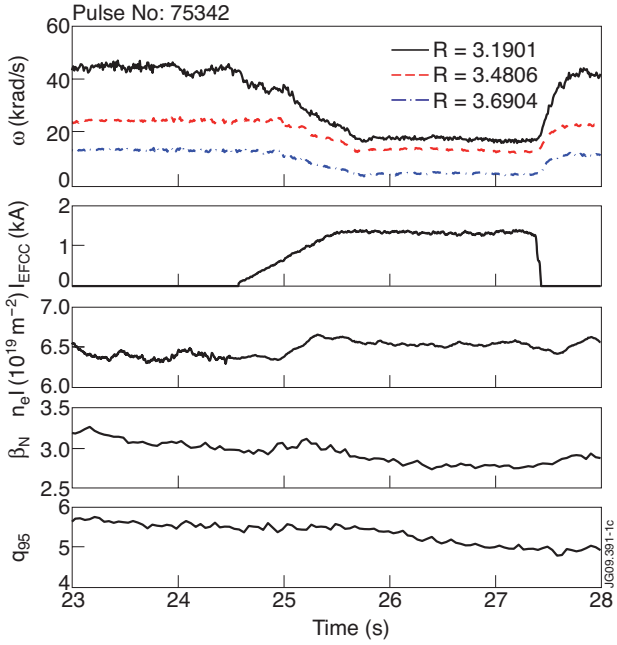

Figure1: From top to bottom, the evolution of the plasma angular rotation frequency at different radii (R=3.19m (ρ~0.09), solid line, R=3.48m (ρ~0.4) dashed line, R=3.69m (ρ~0.73), dashed dotted line, magnetic axis is R0=3.15m), the EFCC current I_{EFCC}, the plasma line-integrated density, the normalized β and q_{95} for JET Pulse No: 75342.

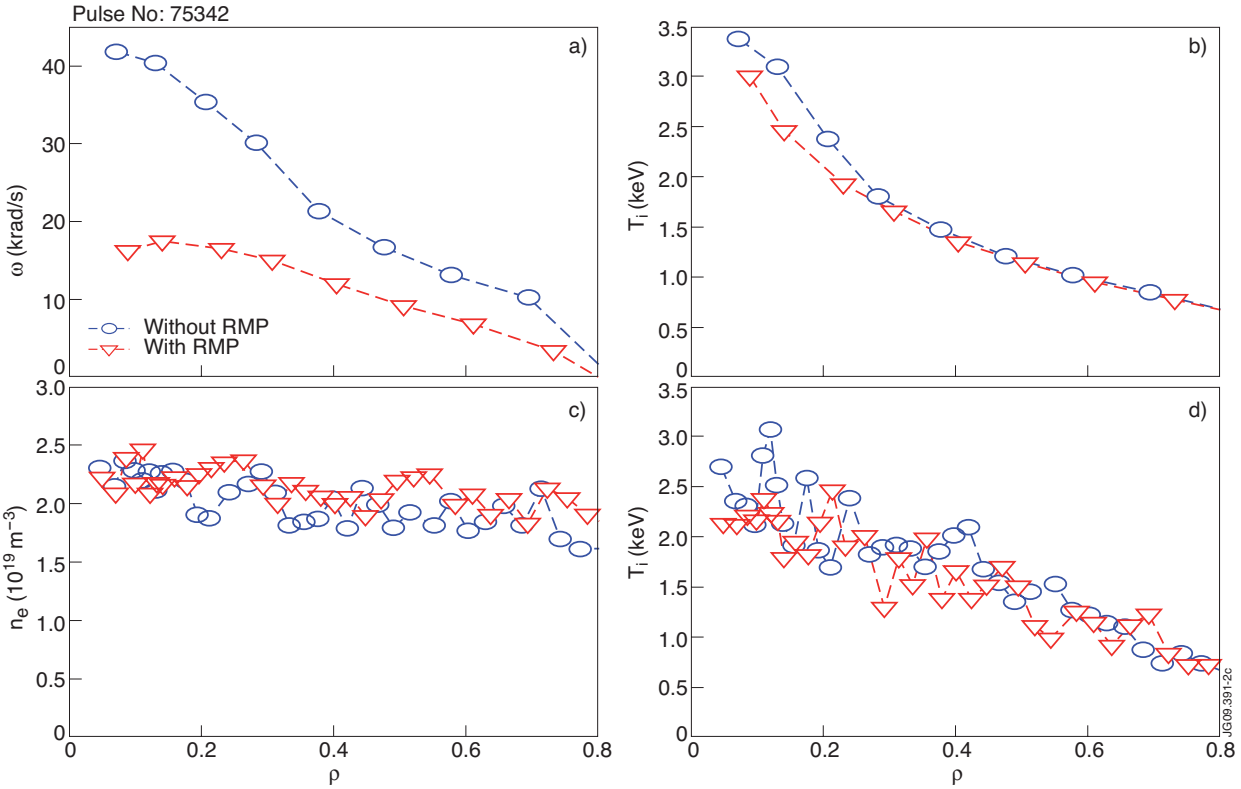

Figure 2: The spatial profiles of (a) the angular rotation frequency, (b) the ion temperature, (c) the electron density and (d) the electron temperature with (circles) and without (triangles) perturbation field, respectively, for JET Pulse No: 75342.

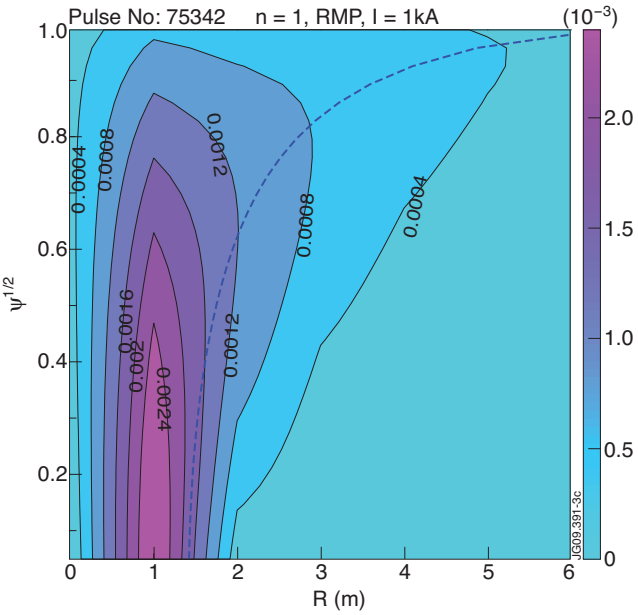

Figure 3: The spectrum of the n = 1 resonant magnetic field perturbation for JET Pulse No: 75342. The dashed line shows the resonant condition m = nq.

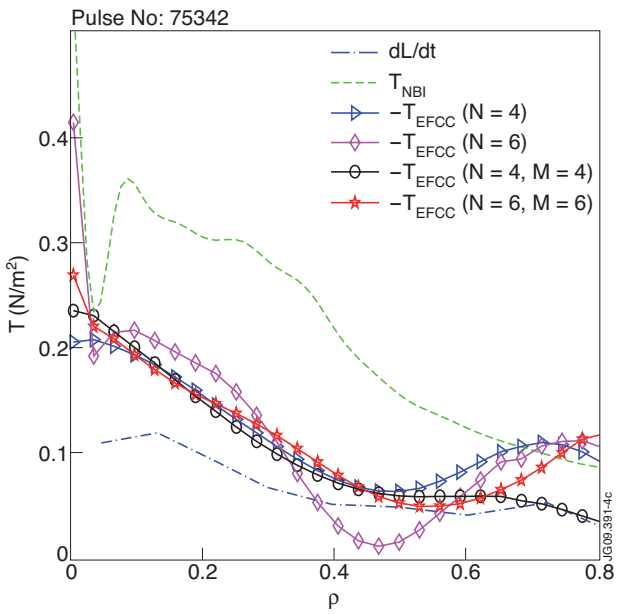

Figure 4: The obtained T_{EFCC} ($-T_{EFCC}$ is plotted) profile by using the χ_M and V_{inwm} profiles fitted from different orders ($N = 4$, triangles, $N = 6$ diamonds, $N = M = 4$, circles, $N = M = 6$, pentacles) of polynomial base functions, the NBI torque (dashed line) and dL/dt (dashed dotted line) at the time just after the switch-off of the EFCC current.

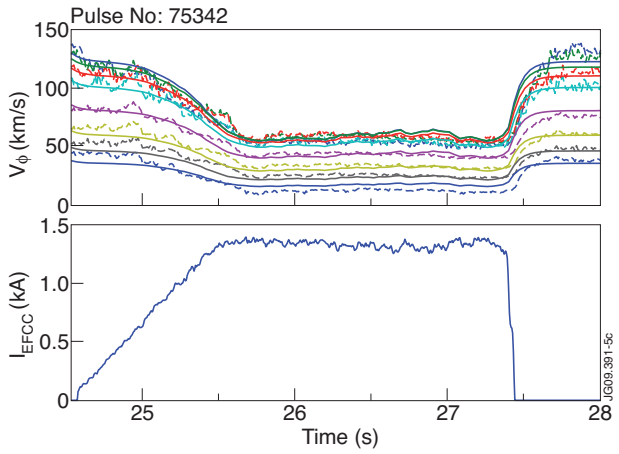

Figure 5: Comparison of the temporal evolution of the plasma velocity (top) between that from the experimental observation (dashed line) and the simulation (solid line). The bottom shows the temporal evolution of the EFCC current

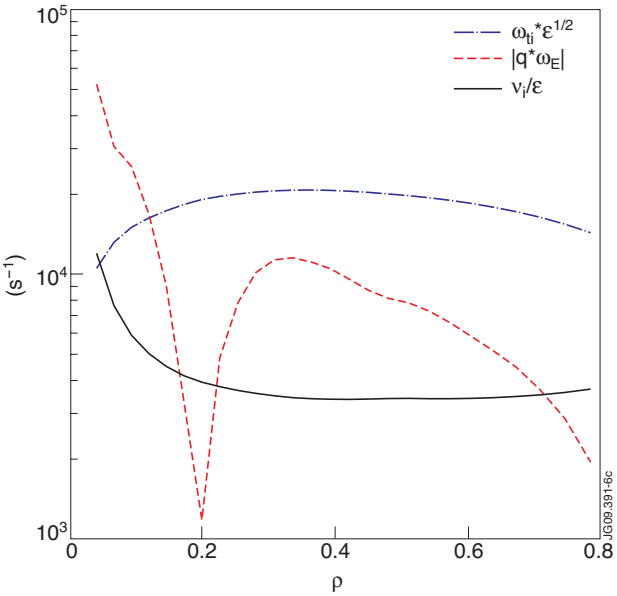

Figure 6: The profiles of the transit ($\varepsilon^{1/2}\,\omega_{ti}$, dotted dashed line), $\vec{E}\times\vec{B}$ drift ($|q\omega_E|$, dashed line) and collision (ν_i/ε, solid line) frequencies for ions.

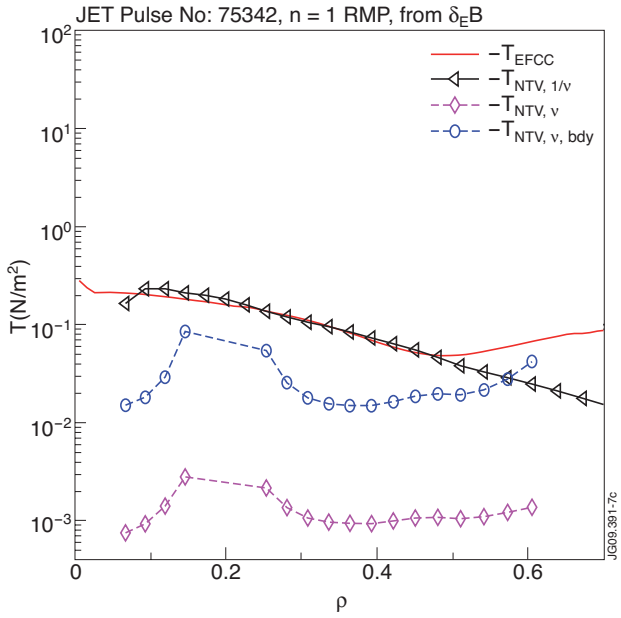

Figure 7: Comparison of the NTV torque profiles from the Eularian variation in the magnetic field strength ($-T_{NTV}$ is plotted, the triangles are the NTV torque in the 1/ν regime, the diamonds are that in the ν regime, the circles are the boundary layer contribution in the ν regime) with the observed torque profile T_{EFCC} ($-T_{EFCC}$ is plotted, solid line, averaged over the four profiles in Figure 4).

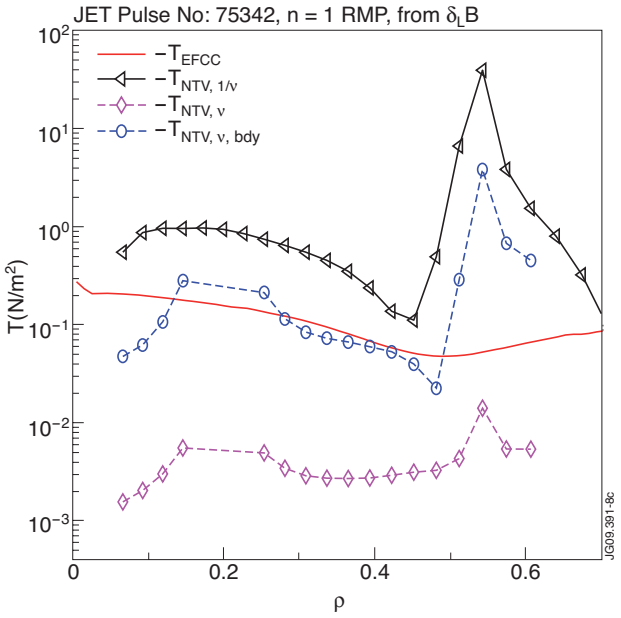

Figure 8: Comparison of the NTV torque profiles from the Lagrangian variation in the magnetic field strength with the observed torque profile T_{EFCC}.

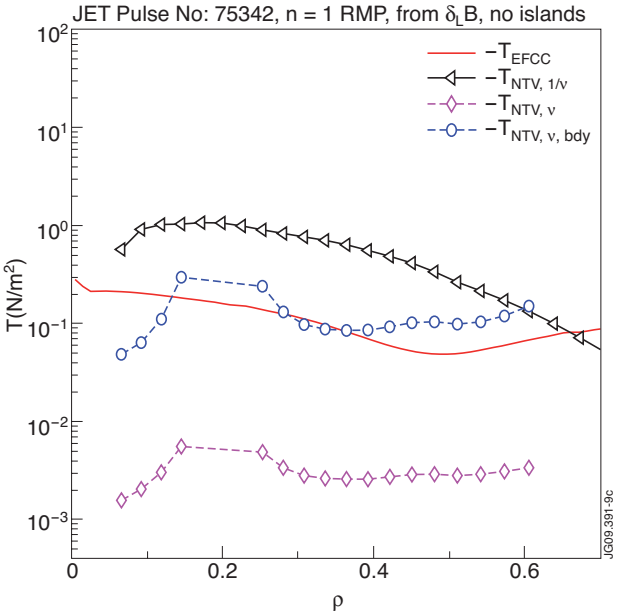

Figure 9: Comparison of the NTV torque profiles from the non-resonant component of the perturbation field with the observed torque profile T_{EFCC}. All the resonant components are assumed to be screened.

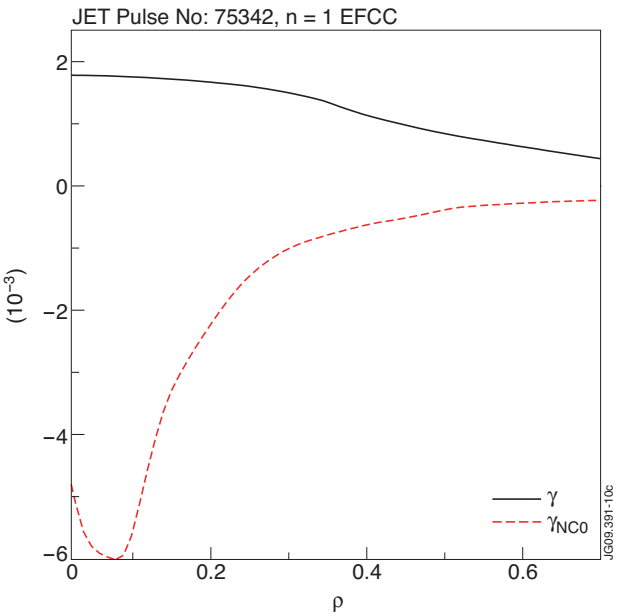

Figure 10: The neoclassical 'offset' angular momentum density ($\gamma_{NC0} \equiv \rho_i V_{NC0}/R$, dashed) in Eq. 5 compared with plasma angular momentum density with perturbation field ($\gamma \equiv \rho_i V_\phi/R$, solid).

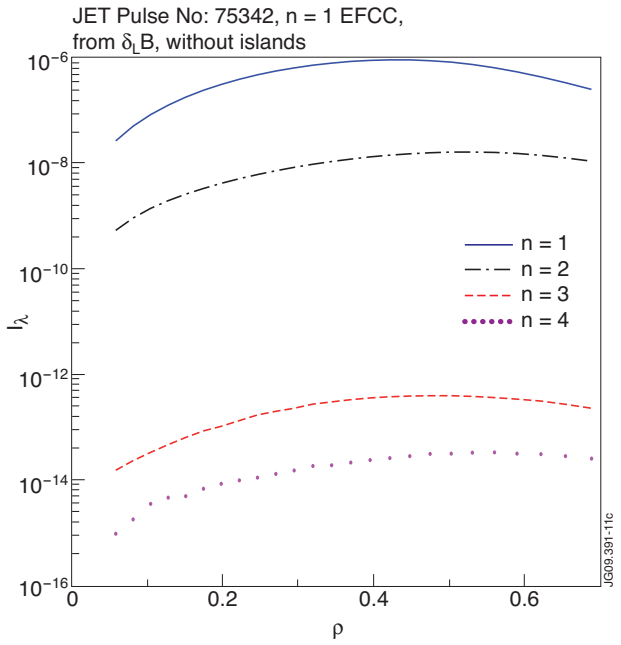

Figure 11: Deferent harmonic's contributions to the pitch angle integration I_λ. The n=1contribution is dominant.

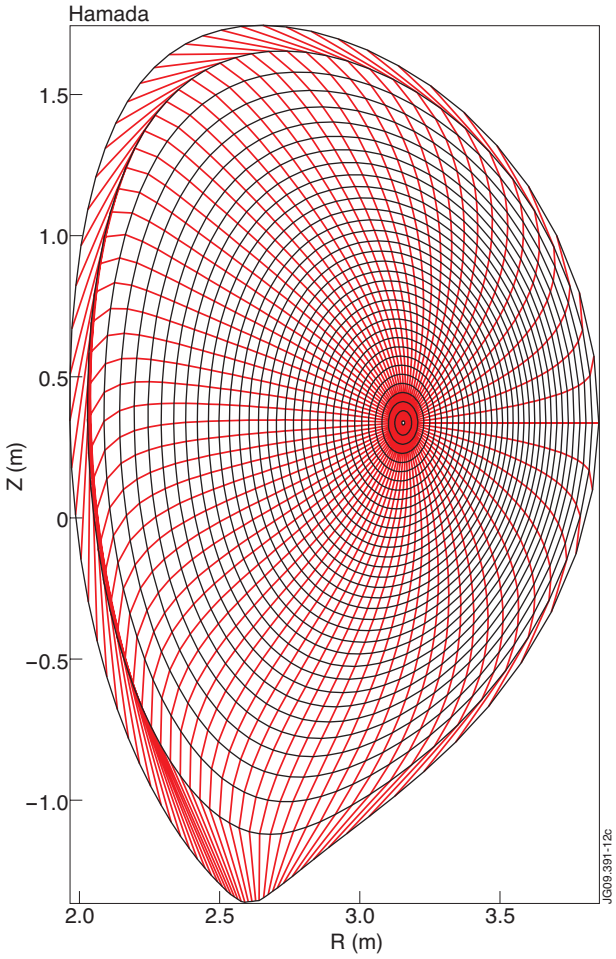

Figure A1: Equally spaced grid ($\sqrt{\psi}$, θ)in Hamada coordinates for JET Pulse No: 75342 at t = 24s.

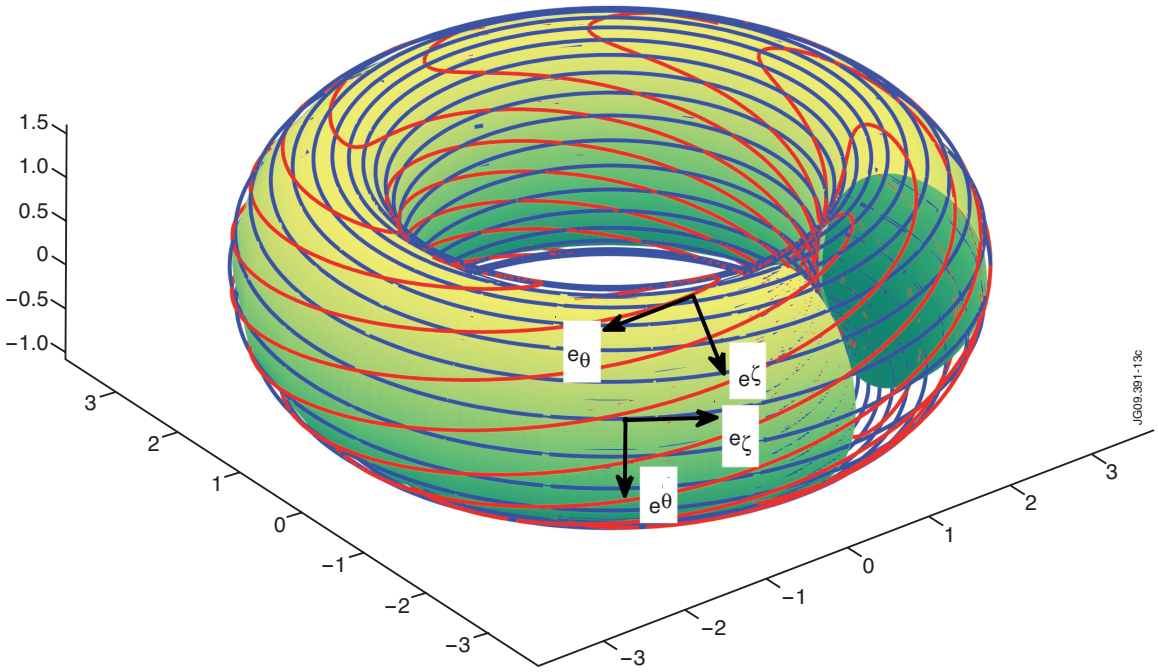

Figure A2. Equally spaced grid (θ, ζ) on the surface $\sqrt{\psi} = 0.95$in Hamada coordinates for JET Pulse No: 75342 at t=24s. The directions of the covariant coordinates (e_θ, e_ζ) and contravariant coordinates (e^θ, e^ζ) are marked in this figure.